

# Nuclear-resonant electron scattering

Adriana Pálffy\* and Zoltán Harman†

*Max-Planck-Institut für Kernphysik,  
Saupfercheckweg 1, 69117 Heidelberg, Germany*

(Dated: April 8, 2008)

## Abstract

We investigate nuclear-resonant electron scattering as occurring in the two-step process of nuclear excitation by electron capture (NEEC) followed by internal conversion. The nuclear excitation and decay are treated by a phenomenological collective model in which nuclear states and transition probabilities are described by experimental parameters. We present capture rates and resonant strengths for a number of heavy ion collision systems considering various scenarios for the resonant electron scattering process. The results show that for certain cases resonant electron scattering can have significantly larger resonance strengths than NEEC followed by the radiative decay of the nucleus. We discuss the impact of our findings on the possible experimental observation of NEEC.

PACS numbers: 34.80.Lx, 34.80.Dp, 23.20.Nx, 23.20.-g

Keywords: electron scattering, nuclear excitation, resonant transitions, highly charged ions

---

\*Electronic address: Palfy@mpi-hd.mpg.de

†Electronic address: Harman@mpi-hd.mpg.de

## I. INTRODUCTION

Electron scattering on ions and atoms provides a valuable experimental means in both atomic and nuclear physics, and is also of great interest due to the significance of this process in high-temperature plasmas (see, for instance, Ref. [1] and references therein). The elastic scattering of free and quasifree electrons on energetic ions has been studied both theoretically [2, 3, 4, 5]) and experimentally [6, 7, 8, 9, 10, 11]. A number of studies have been carried out on electron impact excitation [12, 13, 14, 15, 16] and resonant electron scattering [17, 18, 19]. The latter corresponds to dielectronic capture, i.e., continuum electron capture by the excitation of a bound electron, followed by the Auger decay of the autoionizing state. Since the Auger rates are involved in both steps of this process, the corresponding cross sections are particularly sensitive to the electron-electron interaction. This feature can be used for studies of the relativistic interaction of electrons in the strongest binding nuclear fields available up to now. As an example, the relative contribution of the Breit current-current interaction to the cross section of resonant excitation on hydrogen-like uranium ions was shown to be approximately twice as large as in the case of dielectronic capture followed by radiative de-excitation [19].

Elastic electron scattering provides an indispensable tool for surveying the electromagnetic structure of ground and excited states of nuclei. Electron scattering as a nuclear probe has the major advantage that the interaction is electromagnetic and hence well known. As a result, for a specific charge distribution, the elastic electron scattering cross section can be calculated by phase-shift analysis techniques [20, 21]. As it will be argued in this paper, nuclear-resonant electron scattering in highly charged ions can even provide information about nuclear transitions and excited states via the process of nuclear excitation by electron capture (NEEC).

In the resonant process of NEEC, the collision of a highly charged ion with a free electron with matching kinetic energy leads to a resonant capture into an atomic orbital with the simultaneous excitation of the nucleus [22]. This recombination process was first theoretically proposed by the authors of Ref. [23] in the context of laser-produced plasmas, and is the time-reversed process of internal conversion (IC). Although not yet experimentally observed, NEEC has been an interesting subject after experimental observations of atomic physics processes with regard to the structure of the nucleus have been recently reported,

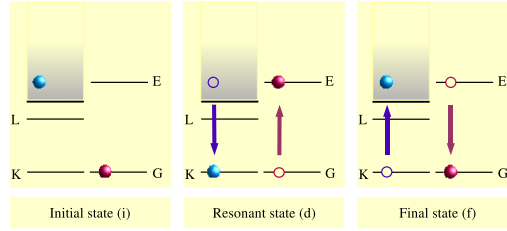


FIG. 1: (Color online) NEEC recombination mechanism of a continuum electron into the  $K$  shell of an initially bare ion, followed by IC of the excited nucleus. The nuclear transition from the ground state  $G$  to the first excited state  $E$  is pictured schematically on the right-hand side of each panel.

such as bound-state internal conversion [24] and its time-reversed process of nuclear excitation by electron transition [25], or the so-called electronic-bridge process, which can be regarded as bound-state internal conversion accompanied by photon emission [26, 27, 28]. Several theoretical studies have been made concerning NEEC in plasmas [23, 29] or in solid targets [30, 31, 32].

As the electron capture in NEEC results in the excitation of the nucleus,  $\gamma$  decay of the nucleus or IC are expected in the second step of the process. Several theoretical aspects of NEEC followed by the radiative decay of the excited nucleus have been recently addressed [22, 33, 34, 35], providing theoretical cross sections and discussing the possible experimental observation of NEEC by detecting the photons emitted in the nuclear  $\gamma$  decay. In this paper we would like to draw the attention to a two-step process in which NEEC is followed by IC, resulting in nuclear-resonant electron scattering (NRES), as schematically pictured in Figure 1.

Our motivation in investigating this electron scattering mechanism is twofold. First, nuclear-resonant electron scattering is far more sensitive to the electron-nucleus interaction than NEEC followed by the radiative decay of the nucleus, due to the presence of the IC rate in each of the two steps of the process. This makes NRES a more suitable candidate for exploring the spectral properties and dynamics of heavy nuclei by the use of experimental methods and facilities primarily developed for atomic physics. Especially, NRES may allow the determination of nuclear transition energies and transition probabilities, the study of atomic vacancy effects on nuclear lifetime [35] and population mechanisms of excited nuclear

levels. A second aspect concerns the experimental observation of NEEC. Theoretical calculations for NEEC followed by IC or radiative decay of the nucleus occurring in scattering measurements are particularly useful in finding candidate isotopes and transitions suitable for experimental observation. For a number of heavy nuclei, the IC rates for low-lying first excited levels are substantially higher than the radiative decay rates, with the immediate consequence that NRES cross sections and resonance strengths are larger than the corresponding values for NEEC followed by the radiative decay of the nucleus. Furthermore, in storage ring experiments aiming at the observation of NEEC by detecting the recombined ions (as in the case of, e.g., dielectronic recombination experiments [36, 37]) both nuclear decay channels should be taken into account. The interest for electron scattering and recombination experiments at the present and future storage ring facilities of the GSI Darmstadt [38, 39] makes nuclear-resonant electron scattering in heavy highly charged ions an important issue for the experimental observation of NEEC.

In this paper we theoretically investigate resonant scattering of electrons undergoing NEEC followed by IC in two possible cases. In the first considered scenario, NEEC and IC occur in the same atomic orbital, as presented schematically in Figure 1. The continuum electron in the initial and final state has then the same kinetic energy in the center-of-mass reference frame. A second possibility considers the case in which the electron is captured into an excited state. NEEC then leads to a doubly-excited intermediate state  $d_1$ , as depicted in Figure 2. This intermediate state can decay via emission of photons from the electron shell or the nucleus, or, alternatively, via IC. Since x-ray emission associated with the electronic de-excitation is faster than nuclear decay of the low-lying excited nuclear states considered here, a second intermediate state  $d_2$  in which the electron is in the ground state is reached. This process was denoted as nuclear excitation by electron capture followed by fast x-ray decay (NEECX) in an earlier work [35], in analogy to the already established notation for the atomic process of resonant transfer and excitation followed by x-ray emission (RTEX). Following NEECX, in the nuclear decay step IC of the excited nucleus occurs if energetically allowed, resulting in a final state characterized by a continuum electron with different kinetic energy than the one in the initial state. We denote the process of NRES with fast x-ray decay of the captured electron by NRESX, in analogy to NEECX and RTEX. This more complicated three-step process is considered because of the advantages for the experiment observation due to the much broader width of the state the electron is captured into, as it

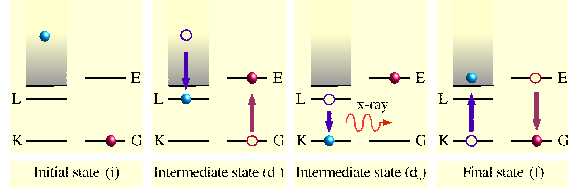


FIG. 2: (Color online) NEEC recombination mechanism of a continuum electron into the  $L$  shell of an initially bare ion, followed by fast x-ray emission from the electronic decay to the  $K$ -shell ground state. The process is completed by IC of the excited nucleus. See text for further explanations.

will be discussed in detail in Section III.

We present total cross sections and resonance strengths for NRES and compare them with the ones presented in Ref. [22, 33] for the case of NEEC followed by the  $\gamma$  decay of the nucleus. The total cross section derivation and a brief description of the electron-nucleus interaction matrix elements are given in Section II. The electric and magnetic electron-nucleus interactions are considered explicitly and the nucleus is described by the help of a nuclear collective model [40]. The dynamics of the electrons is governed by the Dirac equation as required in the case of high- $Z$  elements. Section III presents the numerical results for NRES cross sections and resonance strengths and discusses issues of the possible experimental observation of NEEC. We conclude with a short summary. Atomic units are used throughout this paper unless otherwise specified.

## II. THEORETICAL FORMALISM

In this section we present the total cross section for the process of NEEC followed by IC of the excited nucleus, derived by means of a perturbative expansion of the transition operator. We consider the nuclear transition from the ground state to the first excited state with the simultaneous capture of a free electron into a bare ion or an ion with a closed-subshell configuration. For the cases in which the electron capture does not occur in the ground state, the subsequent fast electronic x-ray decay is taken into account.

### A. Total cross section

The total cross section for NRES can be written with the help of the perturbation expansion of the transition operator, following our formalism presented in Ref. [22]. In order to clearly identify the terms contributing to the process under study, in [22] we introduced Feshbach projection operators that separate the Fock space into subspaces corresponding to the possible initial, intermediate and final states. The initial state of the ion-electron system consisting of the nucleus in its ground state, the free electron, and the vacuum state of the electromagnetic field, can be written as a direct product of the state vectors,

$$|\Psi_i\rangle = |N_i I_i M_i, \vec{p}_i m_{s_i}^+, 0\rangle \equiv |N_i I_i M_i\rangle \otimes |\vec{p}_i m_{s_i}^+\rangle \otimes |0\rangle. \quad (1)$$

Here,  $\vec{p}_i$  is the asymptotic initial momentum of the electron,  $m_{s_i}$  its spin projection, and  $N$  denotes the nuclear ground state, characterized by the angular momentum  $I_i$  and the magnetic quantum number  $M_i$ .

For the two-step process of NEEC followed by IC of the excited nucleus, where the electron capture occurs into the electronic ground state, the intermediate state  $|\Psi_d\rangle$  is given by

$$|\Psi_d\rangle = |N_d I_d M_d, n_d \kappa_d m_d, 0\rangle \equiv |N_d I_d M_d\rangle \otimes |n_d \kappa_d m_d\rangle \otimes |0\rangle, \quad (2)$$

with  $n_d$ ,  $\kappa_d$ , and  $m_d$  being the principal quantum number, Dirac angular momentum, and magnetic quantum number of the bound one-electron state, respectively. The one-electron state is written in the spherical bispinor form

$$\langle \vec{r} | n_d \kappa_d m_d \rangle = \psi_{n_d \kappa_d m_d}(\vec{r}) = \begin{pmatrix} g_{n_d \kappa_d}(r) \Omega_{\kappa_d}^{m_d}(\theta, \varphi) \\ i f_{n_d \kappa_d}(r) \Omega_{-\kappa_d}^{m_d}(\theta, \varphi) \end{pmatrix}, \quad (3)$$

where the  $\Omega_{\kappa_d}^{m_d}$  are the spherical spinors [41] and  $\theta$  and  $\varphi$  are the polar and azimuthal angles associated with the vector  $\vec{r}$ , respectively. The excited nuclear state is denoted by  $|N_d I_d M_d\rangle$ .

The final state for the two-step resonant electron scattering on nuclei is then characterized by the nucleus in its ground state and the electron in the continuum,

$$|\Psi_f\rangle = |N_f I_f M_f, \vec{p}_f m_{s_f}^-, 0\rangle \equiv |N_f I_f M_f\rangle \otimes |\vec{p}_f m_{s_f}^-\rangle \otimes |0\rangle. \quad (4)$$

We denote the energy eigenvalues of the states introduced above as  $E_i$ ,  $E_d$  and  $E_f$ , respectively. Furthermore, the initial and final state continuum electronic wave functions

are given in the coordinate space representation as the partial wave expansion [41]

$$|\vec{p}m_s^\pm\rangle = \sum_{\kappa m m_l} i^l e^{\pm i\Delta_\kappa} Y_{lm_l}^*(\Omega_p) C\left(l \frac{1}{2} j; m_l m_s m\right) |E_c \kappa m\rangle, \quad (5)$$

where  $E_c$  is the energy of the continuum electron measured from the ionization threshold,  $E_c = \sqrt{p^2 c^2 + c^4} - c^2$ . The orbital angular momentum of the partial wave is denoted by  $l$  and the corresponding magnetic quantum number by  $m_l$ . The  $+$ ( $-$ ) sign of the partial wave phases  $\Delta_\kappa$  corresponds to the initial (final) free electron and the phases are chosen so that the continuum wave function fulfills the boundary conditions of an incoming (outgoing) plane wave and an outgoing (incoming) spherical wave. The total angular momentum quantum number of the partial wave is  $j = |\kappa| - \frac{1}{2}$  with its projection  $m = m_l + m_s$  and the symbol  $C(j_1, j_2, j_3; m_1, m_2, m_3)$  stands for the Clebsch-Gordan coefficient. The partial wave functions are represented as

$$\langle \vec{r} | E_c \kappa m \rangle = \psi_{E_c \kappa m}(\vec{r}) = \begin{pmatrix} g_{E_c \kappa}(r) \Omega_\kappa^m(\theta, \varphi) \\ i f_{E_c \kappa}(r) \Omega_{-\kappa}^m(\theta, \varphi) \end{pmatrix}. \quad (6)$$

Following the formalism presented in our previous work [22], the total cross section as a function of the total initial energy  $E$  for the two-step process  $i \rightarrow d \rightarrow f$  is given by

$$\sigma_{i \rightarrow d \rightarrow f}(E) = \frac{2\pi^2}{p^2} \frac{A_{\text{IC}}^{d \rightarrow f} Y_n^{i \rightarrow d}}{\Gamma_d} L_d(E - E_d), \quad (7)$$

where  $A_{\text{IC}}^{d \rightarrow f}$  is the IC decay rate of the nuclear excited state and  $Y_n^{i \rightarrow d}$  the NEEC rate. In the denominator,  $\Gamma_d$  denotes the total natural line width of the nuclear excited state, given by the sum of the partial IC and  $\gamma$  decay widths,  $\Gamma_d = \Gamma_{\text{IC}} + \Gamma_\gamma$ . The continuum electron energy dependence is given by the well-known Lorentz line profile function

$$L_d(E_c - E_{\text{exc}} - \varepsilon_{n_d \kappa_d}) = L_d(E - E_d) = \frac{\Gamma_d/2\pi}{(E - E_d)^2 + \frac{1}{4}\Gamma_d^2} \quad (8)$$

with the width  $\Gamma_d$  given by the natural width of the excited nuclear state. Here we introduced the notation  $E_{\text{exc}}$  for the nuclear excitation energy and  $\varepsilon_{n_d \kappa_d}$  for the energy of the bound intermediate electronic state. The cross section formula (7) is valid in the resonant case, i.e. for continuum electron energies  $E_c$  approximately fulfilling the resonance condition  $E_c = E_{\text{exc}} + \varepsilon_{n_d \kappa_d}$ .

Since NEEC is the time-reversed process of IC, and we consider cases involving transitions between two nuclear levels only, the rates of the two processes occurring between the states

$d$  and  $f$  and  $i$  and  $d$  can be related by the principle of detailed balance,

$$A_{\text{IC}}^{d \rightarrow f} = \frac{2(2I_i + 1)}{(2I_d + 1)(2j_d + 1)} Y_n^{i \rightarrow d}, \quad (9)$$

where  $j_d$  denotes the total angular momentum of the bound electron.

For the resonant three-step process depicted in Figure 2, in which NEEC occurs into an excited electronic state with subsequent fast x-ray emission, the first intermediate state given in Eq. (2) becomes

$$\begin{aligned} |\Psi_{d_1}\rangle &= |N_d I_d M_d, n_d^* \kappa_d^* m_d^*, 0\rangle \\ &\equiv |N_d I_d M_d\rangle \otimes |n_d^* \kappa_d^* m_d^*\rangle \otimes |0\rangle, \end{aligned} \quad (10)$$

where  $n_d^*$ ,  $\kappa_d^*$  and  $m_d^*$  are the quantum numbers of the excited electronic state. The second intermediate state following the fast x-ray electronic decay is characterized by the electron in the ground state, the excited nucleus and a photon with wavenumber  $\vec{k}$  and polarization  $\nu = 1, 2$ ,

$$\begin{aligned} |\Psi_{d_2}\rangle &= |N_d I_d M_d, n_d \kappa_d m_d, \vec{k} \nu\rangle \\ &\equiv |N_d I_d M_d\rangle \otimes |n_d \kappa_d m_d\rangle \otimes |\vec{k} \nu\rangle. \end{aligned} \quad (11)$$

The photon is emitted in the x-ray decay of the electron from the excited state  $|n_d^* \kappa_d^* m_d^*\rangle$  to the ground state  $|n_d \kappa_d m_d\rangle$ . The projection operator formalism presented in Ref. [22] is extended to account for the emission of such a photon. The corresponding total cross section for the three-step process  $i \rightarrow d_1 \rightarrow d_2 \rightarrow f$  can be written as

$$\sigma_{i \rightarrow d_1 \rightarrow d_2 \rightarrow f}(E) = \frac{2\pi^2}{p^2} \frac{A_{\text{IC}}^{d_2 \rightarrow f}}{\Gamma_{d_2}} \frac{A_{\text{x-ray}}^{d_1 \rightarrow d_2}}{\Gamma_{d_1}} Y_n^{i \rightarrow d_1} L_{d_1}(E - E_{d_1}), \quad (12)$$

where  $A_{\text{x-ray}}$  is the electronic radiative decay rate and  $\Gamma_{d_1}$  and  $\Gamma_{d_2}$  are the widths of the two intermediate states. The width  $\Gamma_{d_1}$  of the doubly-excited state  $d_1$  is given as the sum of the nuclear and electronic widths,  $\Gamma_{d_1} = \Gamma_\gamma + \Gamma_{\text{IC}} + \Gamma_{\text{x-ray}}$ , and can be approximated as  $\Gamma_{d_1} \simeq \Gamma_{\text{x-ray}}$  due to the difference of magnitude of the electronic and nuclear widths. The natural width of the nuclear excited state determines the width of the second intermediate state  $\Gamma_{d_2}$ . The Lorentz profile is characterized in this case by the width of the first intermediate state,  $\Gamma_{d_1} \simeq \Gamma_{\text{x-ray}}$ . Because of the large lifetime of the nuclear excited state, in Eq. (12) an additional second term standing for the process in which the nuclear decay occurs prior to the electronic decay can be neglected.



The integration of the cross section over the continuum electron energy gives the resonance strength  $S$  for a given capture process. In the case of the two-step process  $i \rightarrow d \rightarrow f$  described by the total cross section in Eq. (7), the continuum electron momentum  $p$  and thus the NEEC rate  $Y_n^{i \rightarrow d}$  are practically constant in the energy interval defined by the very narrow nuclear width. Since the Lorentz function is normalized to unity, the resonance strength can be written as

$$S = \frac{2\pi^2}{p^2} \frac{A_{\text{IC}}^{d \rightarrow f} Y_n^{i \rightarrow d}}{\Gamma_d}. \quad (13)$$

For the more complicated three-step process involving NEEC into an excited electronic state followed by x-ray emission and IC of the captured electron, the resonance strength is obtained by integrating the total cross section given in Eq. (12), and has the expression

$$S = \frac{2\pi^2}{p^2} \frac{A_{\text{IC}}^{d_2 \rightarrow f}}{\Gamma_{d_2}} \frac{A_{\text{x-ray}}^{d_1 \rightarrow d_2}}{\Gamma_{d_1}} Y_n^{i \rightarrow d_1}. \quad (14)$$

Similarly, since the transition width  $\Gamma_{d_1}$  is still much smaller than the continuum electron energy, we have assumed here resonance values for the momentum  $p$  and the NEEC rate  $Y_n^{i \rightarrow d}$ .

## B. The electron-nucleus interaction

The NEEC rates in Eqs. (7) and (12) are proportional to the squared matrix elements of the electric and magnetic electron-nucleus interactions and have the expression [22]

$$Y_n^{i \rightarrow d} = \frac{2\pi}{2(2I_i + 1)} \sum_{M_i m_{s_i}} \sum_{M_d m_d} \int d\Omega_p \rho_i \times |\langle N_d I_d M_d, n_d \kappa_d m_d, 0 | H_{en} + H_{magn} | N_i I_i M_i, \vec{p}_i m_{s_i}^+, 0 \rangle|^2. \quad (15)$$

Here, the integral is performed over the incoming electron direction  $\Omega_p$  and  $\rho_i$  denotes the density of the electronic continuum states ( $\rho_i = 1$  in the units applied here). The electron-nucleus interaction Hamiltonians  $H_{en}$  and  $H_{magn}$  describe the electric and magnetic transitions of the nucleus, respectively. We adopt the Coulomb gauge for the electron-nucleus interaction  $H_{en}$ , since it allows the separation of the dominant Coulomb attraction between the electronic and nuclear degrees of freedom,

$$H_{en} = \int d^3 r_n \frac{\rho_n(\vec{r}_n)}{|\vec{r}_e - \vec{r}_n|}. \quad (16)$$

Here,  $\rho_n(\vec{r}_n)$  is the nuclear charge density and the integration is performed over the whole nuclear volume. The magnetic interaction Hamiltonian accounts for the recombination of the free electron by exchanging a virtual transverse photon. In the limit of long exchange photon wavelength, the magnetic interaction Hamiltonian is approximated by

$$H_{magn} = -\frac{1}{c}\vec{\alpha} \int d^3r_n \frac{\vec{j}_n(\vec{r}_n)}{|\vec{r} - \vec{r}_n|}, \quad (17)$$

where  $\vec{j}_n(\vec{r}_n)$  is the nuclear current vector and  $\vec{\alpha}$  is the vector of Dirac matrices.

For describing the nucleus we use a collective model [40] in which the excitations of the nucleus are assumed to be vibrations or rotations of the nuclear surface. The expressions of the nuclear charge density and current in the two interaction Hamiltonians can then be written in terms of nuclear collective coordinates by means of a nuclear surface parameterization. Since the details of the calculation of the interaction Hamiltonian matrix elements are given elsewhere [22, 33], here we only present their final expressions. The NEEC transition probability per unit time is given by

$$Y_n^{(e)} = \frac{4\pi^2\rho_i}{(2L+1)^2} B(EL, I_i \rightarrow I_d)(2j_d + 1) \quad (18)$$

$$\times \sum_{\kappa} |R_{L,\kappa_d,\kappa}^{(e)}|^2 (2j+1) \begin{pmatrix} j_d & j & L \\ \frac{1}{2} & -\frac{1}{2} & 0 \end{pmatrix}^2,$$

for electric transitions of multipolarity  $L$ . The quantity

$$B(\lambda L, I_i \rightarrow I_d) = \frac{1}{2I_i + 1} |\langle N^* I_d || \mathcal{M}_L || N I_i \rangle|^2 \quad (19)$$

represents the reduced nuclear transition probability, where  $\lambda$  stands for electric ( $E$ ) or magnetic ( $M$ ) and  $\mathcal{M}$  is the corresponding multipole moment operator. We have denoted by  $R_{L,\kappa_d,\kappa}^{(e)}$  the electronic matrix element

$$R_{L,\kappa_d,\kappa}^{(e)} = \int_0^\infty dr r^{-L+1} \left( f_{n_d\kappa_d}(r) f_{E_c\kappa}(r) + g_{n_d\kappa_d}(r) g_{E_c\kappa}(r) \right), \quad (20)$$

where  $g_{E_c\kappa}(r)$  and  $f_{E_c\kappa}(r)$  are the large and small radial components of the relativistic continuum electron wave function in Eq. (6), respectively, and  $g_{n_d\kappa_d}(r)$  and  $f_{n_d\kappa_d}(r)$  are the corresponding components of the bound Dirac wave functions as in Eq. (3). The last factor in the summand of Eq. (18) is a 3- $j$  symbol. For magnetic transitions of multipolarity  $L$ ,

the NEEC rate has the expression

$$Y_n^{(m)} = \frac{4\pi^2 \rho_i}{L^2(2L+1)^2} B(ML, I_i \rightarrow I_d)(2j_d + 1) \times \sum_{\kappa} \left| R_{L, \kappa_d, \kappa}^{(m)} \right|^2 (2j+1)(\kappa_d + \kappa) \begin{pmatrix} j_d & j & L \\ \frac{1}{2} & -\frac{1}{2} & 0 \end{pmatrix}^2, \quad (21)$$

where we introduced the following notation for the radial integral:

$$R_{L, \kappa_d, \kappa}^{(m)} = \int_0^\infty dr r^{-L+1} \left( g_{n_d \kappa_d}(r) f_{E_c \kappa}(r) + f_{n_d \kappa_d}(r) g_{E_c \kappa}(r) \right). \quad (22)$$

The radial expressions  $R_{L, \kappa_d, \kappa}^{(e)}$  and  $R_{L, \kappa_d, \kappa}^{(m)}$  are integrated numerically.

### III. NUMERICAL RESULTS

We calculate NRES total cross sections and resonance strengths for a number of systems involving highly charged ions of stable or long-lived ground state isotopes. In the first place we investigate the two-step process of NRES in which electron capture occurs into the electronic ground state and consequently the NEEC and IC bound electronic states coincide, as depicted in Figure 1. NEEC occurring in bare ions is considered for  $E2$  transitions from the  $0^+$  ground states to the first  $2^+$  excited nuclear states of  $^{154}_{64}\text{Gd}$ ,  $^{164}_{66}\text{Dy}$ ,  $^{170}_{68}\text{Er}$ ,  $^{174}_{70}\text{Yb}$ ,  $^{178}_{72}\text{Hf}$  and  $^{180}_{74}\text{W}$ . The energies of the excited nuclear levels  $E_{\text{exc}}$  as well as the reduced transition probabilities  $B(E2)$ , needed for the calculation of the natural width of the nuclear excited state and the NEEC rate, are taken from Ref. [42]. The  $M1$  transitions between the ground states and the first excited states of  $^{155}_{64}\text{Gd}$ ,  $^{165}_{67}\text{Ho}$ ,  $^{173}_{70}\text{Yb}$ ,  $^{175}_{71}\text{Lu}$ ,  $^{179}_{72}\text{Hf}$ ,  $^{185}_{75}\text{Re}$  and  $^{187}_{75}\text{Re}$  are also considered. For these cases, the dominant  $M1$  multipolarity is accompanied by a weaker  $E2$  component. For the NEEC and IC rates, we take into account the multipole mixing by considering both Hamiltonians  $H_{en}$  corresponding to the  $E2$  transition and  $H_{magn}$  corresponding to the  $M1$  transition in Eq. (15). Due to the specific parity of the electronic wavefunction components, the mixed terms in Eq. (15) vanish and the NEEC rate can be written as a sum of the partial NEEC rates for the separate  $M1$  and  $E2$  multipolarities. A similar result is obtained for the  $\gamma$  decay rate of a mixed multipole transition. The nuclear data for the magnetic transitions were taken from [43, 44, 45, 46, 47, 48, 49].

In the following we compare NRES, i.e., NEEC followed by IC, with the case when the excited nuclear state occurring in NEEC decays radiatively. Resonance strengths for both

scenarios involving electronic capture into the  $K$  shell of a bare ion are compared in Table I. The resonance strengths are indexed according to the nuclear decay channel as  $S_{\text{IC}}$  and  $S_\gamma$ . In the case of NEEC followed by the  $\gamma$  decay of the nucleus, the resonance strength is given by [22]

$$S_\gamma = \frac{2\pi^2}{p^2} \frac{A_\gamma^{d \rightarrow f} Y_n^{i \rightarrow d}}{\Gamma_d}, \quad (23)$$

where  $A_\gamma^{d \rightarrow f}$  is the nuclear  $\gamma$  decay rate, related to the reduced transition probability  $B$  and nuclear excitation energy  $E_{\text{exc}}$  by [50]

$$A_\gamma^{d \rightarrow f} = \frac{8\pi(L+1)}{L[(2L+1)!!]^2} (E_{\text{exc}})^{2L+1} B(\lambda L, I_e \rightarrow I_g). \quad (24)$$

For the calculation of the NEEC and IC rates, the numerical evaluation of the radial integrals  $R_{L,\kappa_d,\kappa}$  [see Eqs. (20) and (22)] is needed. We consider Coulomb-Dirac wave functions for the continuum electron and wave functions calculated with the GRASP92 package [51] assuming the potential of a homogeneously charged nucleus for the bound electron. The value of  $R_{L,\kappa_d,\kappa}$  is not affected by finite nuclear size effects on the accuracy level of our calculations. Nevertheless, the finite size of the nucleus has a sensitive effect on the energy levels of the bound electron. The energy of the bound electronic state is calculated with GRASP92 and includes one-loop one-electron quantum electrodynamic (QED) terms, and in the case of many-electron bound states approximate QED screening corrections.

The comparison in Table I shows that the resonance strengths for NRES and for NEEC followed by  $\gamma$  emission are typically on the same order of magnitude. For  $E2$  transitions, the  $\gamma$  decay of the excited nuclear state tends to dominate over the IC decay, so that  $S_{\text{IC}} < S_\gamma$ . For magnetic dipole transitions, typically the NRES resonance strength values are larger than the ones for NEEC followed by  $\gamma$  emission, culminating with the case of  $^{155}_{64}\text{Gd}$ , for which  $S_{\text{IC}}=8.48$  b eV and  $S_\gamma=2.19$  b eV. The difference between  $S_{\text{IC}}$  and  $S_\gamma$  is given by the decay channel only, namely, by the decay rates of the nuclear excited state  $A_{\text{IC}}$  and  $A_\gamma$ , respectively. The ratio  $\alpha = A_{\text{IC}}/A_\gamma$  denotes the IC coefficient, whose values are calculated for a particular bound shell or orbital. The behaviour of  $\alpha$  with respect to the capture orbital depends on the multipolarity of the nuclear transition. While for  $E2$  transitions  $p$  orbitals have larger  $\alpha$  values, for  $M1$  transitions the  $s$  orbitals have a stronger contribution to the total IC coefficient. It is therefore not surprising that in Table I, with resonance strengths considering NEEC into the  $1s_{1/2}$  orbital of bare ions, for  $M1$  transitions the NRES resonance strengths are typically larger than the ones for NEEC followed by  $\gamma$  decay,  $S_{\text{IC}} \gtrsim S_\gamma$ . In

TABLE I: Resonance strength comparison between NRES ( $S_{\text{IC}}$ ) and NEEC followed by  $\gamma$  decay ( $S_\gamma$ ) for various heavy ion collision systems involving capture of the free electron in the  $1s_{1/2}$  orbital of bare ions. The nuclear excitation energy  $E_{\text{exc}}$ , the continuum electron energy at resonance in the center-of-mass frame  $E_c$ , and the multipolarity of the transition  $L$  are given in the second, third and fourth column, respectively.

Isotope	$E_{\text{exc}}$ (keV)	$E_c$ (keV)	$L$	$S_{\text{IC}}$ (b eV)	$S_\gamma$ (b eV)
$^{154}_{64}\text{Gd}$	123.071	64.005	$E2$	$1.21 \times 10^{-2}$	$2.87 \times 10^{-2}$
$^{164}_{66}\text{Dy}$	73.392	10.318	$E2$	$4.93 \times 10^{-2}$	$3.86 \times 10^{-2}$
$^{170}_{68}\text{Er}$	78.591	11.350	$E2$	$4.90 \times 10^{-2}$	$4.69 \times 10^{-2}$
$^{174}_{70}\text{Yb}$	76.471	4.897	$E2$	$3.39 \times 10^{-3}$	$3.61 \times 10^{-3}$
$^{178}_{72}\text{Hf}$	93.180	17.103	$E2$	$3.11 \times 10^{-2}$	$4.64 \times 10^{-2}$
$^{180}_{74}\text{W}$	103.557	22.776	$E2$	$2.30 \times 10^{-2}$	$4.41 \times 10^{-2}$
$^{155}_{64}\text{Gd}$	60.008	0.942	$M1 + E2$	8.48	2.19
$^{165}_{67}\text{Ho}$	94.700	29.563	$M1 + E2$	1.19	0.88
$^{173}_{70}\text{Yb}$	78.647	7.073	$M1 + E2$	3.85	1.31
$^{175}_{71}\text{Lu}$	113.804	40.002	$M1 + E2$	0.153	0.151
$^{179}_{72}\text{Hf}$	122.7909	46.714	$M1 + E2$	0.327	0.348
$^{185}_{75}\text{Re}$	125.358	42.198	$M1 + E2$	1.74	1.47
$^{187}_{75}\text{Re}$	134.243	51.083	$M1 + E2$	1.15	1.18

addition, the NRES resonance strengths for  $M1$  transitions are substantially larger than the ones for  $E2$  transitions, also due to the broader natural line widths of the former.

For heavier even-even nuclei such as the actinides  $^{232}_{90}\text{Th}$ ,  $^{236}_{92}\text{U}$ ,  $^{238}_{92}\text{U}$ , and  $^{248}_{96}\text{Cm}$ , the capture into the  $K$  shell is not possible since the binding energy of the  $1s_{1/2}$  electron is larger than the nuclear excitation energy. These nuclei present first-excited  $2^+$  states lying at about 40 keV above the  $0^+$  ground state. Due to their low transition energies and large corresponding IC coefficients, the actinide nuclei are prospective candidates for NRES with recombination into the  $L$  shell. In Table II, we consider NEEC with capture into the  $2s_{1/2}$ ,  $2p_{1/2}$  and  $2p_{3/2}$  orbitals of the ground state electronic configuration of the He-like ( $1s^2_{1/2}$ ), Be-like ( $1s^2_{1/2}2s^2_{1/2}$ ) and C-like ( $1s^2_{1/2}2s^2_{1/2}2p^2_{1/2}$ ) ions, respectively. NRES resonance strengths are compared to the ones of NEEC followed by  $\gamma$  decay of the nucleus. Unlike the cases of

NEEC occurring in bare ions, in this case the width of the nuclear excited state may also contain terms corresponding to the IC decay of the bound electrons in the initial electronic configuration. The presence of the  $K$ -shell electrons does not play any role in the nuclear decay, since the low energy of the nuclear transition does not allow their IC. For Be-like and C-like ions, however, the IC decay rates of the  $2s_{1/2}$  and  $2p_{1/2}$  orbital electrons contribute to the total width of the nuclear excited state. For the calculation of the radial wave functions for the continuum electron, we assume a total screening of the nuclear charge, i.e., we use Coulomb-Dirac functions with an effective nuclear charge  $Z_{\text{eff}} = Z - N$ , where  $N$  stands for the number of bound electrons. For the bound electron wave functions, the electron-electron interaction is accounted for in the Dirac-Fock approximation.

TABLE II: Resonance strength comparison between NRES ( $S_{\text{IC}}$ ) and NEEC followed by  $\gamma$  decay ( $S_\gamma$ ) for several heavy ion collision systems involving capture of the free electron in the  $2s_{1/2}$  orbital of He-like ions, the  $2p_{1/2}$  orbital of Be-like ions and the  $2p_{3/2}$  orbital of C-like ions. The nuclear excitation energy  $E_{\text{exc}}$ , the continuum electron energy at resonance in the center-of-mass frame  $E_c$ , and the capture orbital  $nl_j$  are given in the second, third and fourth column, respectively.

Isotope	$E_{\text{exc}}(\text{keV})$	$E_c(\text{keV})$	$nl_j$	$S_{\text{IC}} \text{ (b eV)}$	$S_\gamma \text{ (b eV)}$
$^{232}_{90}\text{Th}$	49.369	18.244	$2s_{1/2}$	0.011	$5.44 \times 10^{-3}$
		19.400	$2p_{1/2}$	0.416	$6.93 \times 10^{-3}$
		24.010	$2p_{3/2}$	0.055	$1.95 \times 10^{-3}$
$^{236}_{92}\text{U}$	45.242	12.405	$2s_{1/2}$	0.033	$7.99 \times 10^{-3}$
		13.596	$2p_{1/2}$	0.906	$8.32 \times 10^{-3}$
		19.655	$2p_{3/2}$	0.098	$1.97 \times 10^{-3}$
$^{238}_{92}\text{U}$	44.916	12.073	$2s_{1/2}$	0.039	$9.06 \times 10^{-3}$
		13.262	$2p_{1/2}$	1.055	$9.35 \times 10^{-3}$
		18.323	$2p_{3/2}$	0.120	$2.32 \times 10^{-3}$
$^{248}_{96}\text{Cm}$	43.380	6.888	$2s_{1/2}$	0.147	$1.79 \times 10^{-2}$
		8.190	$2p_{1/2}$	2.936	$1.55 \times 10^{-2}$
		14.203	$2p_{3/2}$	0.240	$2.94 \times 10^{-3}$

We find that NRES resonance strengths for electron capture and scattering on the  $2p$

orbitals are up to two orders of magnitude larger than the corresponding values for NEEC followed by  $\gamma$  decay of the nucleus for the highly charged actinides presented in Table II. The  $2p$  orbitals of  $^{232}_{90}\text{Th}$ ,  $^{236}_{92}\text{U}$ ,  $^{238}_{92}\text{U}$  and  $^{248}_{96}\text{Cm}$  have a major role in the IC decay of the excited nuclear state. The IC coefficients corresponding to the neutral atom have values between  $\alpha = 327$  for the transition of  $^{232}_{90}\text{Th}$  and  $\alpha = 984$  for the one of  $^{248}_{96}\text{Cm}$ . In few-electron configurations, however, the strongly-bound inner-shell electrons have a more pronounced influence on nuclear coupling to the atomic shells [52]. One electron in the  $2p_{1/2}$  orbital of the highly charged ion of  $^{248}_{96}\text{Cm}$ , for instance, accounts already for a partial IC coefficient of  $\alpha = 188$ . Thus the two orders of magnitude difference between  $S_{\text{IC}}$  and  $S_{\gamma}$  in Table II can be traced back to the behaviour of the IC and radiative decay rates and the IC coefficient. The relatively small energy of the nuclear transitions leads to a low radiative decay rate. On the other hand, the heavy actinides presented in Table II are high- $Z$  nuclei with large radial electronic integrals  $R_{L,\kappa_d,\kappa}$  which lead to significant IC rates. The largest NRES resonance strength is associated with capture into the  $2p_{1/2}$  orbital of  $^{248}_{96}\text{Cm}$ , with  $S_{\text{IC}} = 2.94 \text{ b eV}$ , which is on the same order of magnitude with the corresponding values presented in Table I for  $M1$  nuclear transitions.

In the scenario considered so far, only few electrons fulfill the resonance condition due to the very narrow natural width of the nuclear excited state. A possibility to relax the resonance condition is given by the capture of the electron into an excited bound state. We consider therefore the more complicated three-step NRESX process depicted in Figure 2, in which NEEC into an excited electronic state is followed by  $K\alpha$  x-ray emission and only subsequently by IC of the captured electron. Since the capture and IC electronic states do not coincide, the scattered free electron will have a different kinetic energy than the incident electronic beam, with the difference in energy being carried away by the x-ray photon. Furthermore, for the very heavy actinide nuclei where the electron capture into the  $K$  shell with the excitation of the first collective excited level is not possible, NRESX among  $L$  subshells turns out to have several advantages for experimental observation. The resonance strength for NRESX is calculated using the expression in Eq. (14), where the required electronic widths and x-ray transition rates are provided by the OSCL92 module of the GRASP92 package.

For the first group of isotopes in Table I, where capture into and, consequently, IC from the  $K$  shell is possible, we envisage NEEC into the  $L$  shell of bare ions. The x-ray decay

of the captured electron to the  $K$  shell occurs orders of magnitude faster than the nuclear de-excitation. In this case, the IC decay of the nucleus will follow the x-ray emission and will ionize the bound electron from the  $K$  shell. In Tables III and IV we present continuum electron energies  $E_c$ , NEEC rates  $Y_n$  and NRESX resonance strengths  $S$  for the capture into the  $2s_{1/2}$ ,  $2p_{1/2}$  and  $2p_{3/2}$  orbitals of bare ions. Compared to the resonance strengths for the two-step process of NRES presented in Table I, the values for NRESX are several orders of magnitude smaller. The main reason for this behaviour is the dependence of the resonance strength on the momentum of the incoming continuum electron  $p$ , presented in Eq. (12). All isotopes in Tables III and IV have nuclear excitation energies that allow NEEC into the  $K$  shell. Since the capture occurs however into the  $L$  shell, the continuum electron energy at the resonance has large values, starting from the energy difference between the  $L$  and  $K$  shells. As shown in the third column of Tables III and IV, the continuum electron energy has values between approximately 45 keV for the case of  $^{155}_{64}\text{Gd}$  and going up to 114 keV for  $^{187}_{75}\text{Re}$ .

The case of the heavy actinide nuclei with low-lying first excited states also offers other scenarios for NRESX. Since IC of the  $K$ -shell electrons is energetically forbidden, we consider in the following capture into initially He-like ions. A first scenario considers NEEC into the  $2p$  orbitals of He-like ions, followed by the fast x-ray decay of the captured electron to the  $2s_{1/2}$  state. The x-ray transition for the considered highly charged ions occurs several orders of magnitude faster than the nuclear decay. IC will therefore follow the electronic transition and ionize the  $2s_{1/2}$  electron. The initial and final continuum electron energies are then given by the corresponding energies of the IC and capture  $L$  subshells. In a similar manner, one can envisage the NEEC into the  $3p$  orbitals of He-like ions, with the subsequent decay of the captured electron to the  $2s$  ground state. In Table V we present continuum electron energies and NRESX resonance strengths for NEEC occurring into the  $2p$  and  $3p$  orbitals of He-like  $\text{Th}^{88+}$ ,  $\text{U}^{90+}$ , and  $\text{Cm}^{94+}$  ions. The resonance strengths for NEEC into the  $2p$  orbitals are larger than the ones for capture into the  $3p$  orbitals, due to the smaller electron momentum values and different overlap of the electronic wave functions with the nuclear matter. The largest resonance strength value is the one for NRESX with capture into the  $2p_{1/2}$  orbital of the initially He-like  $\text{Cm}^{94+}$  ion, namely,  $S = 3.41 \text{ b eV}$ .

The initial and final states of NRESX coincide with those of bremsstrahlung, where a photon is directly emitted in a continuum-continuum transition. Bremsstrahlung is therefore



TABLE III: Resonance strengths  $S$  for NRESX: electron recombination into the  $L$  shell orbitals of bare ions followed by  $K$ -shell IC. The nuclear transition multipolarity is  $E2$ .  $E_{\text{exc}}$  denotes the nuclear excitation energy,  $E_c$  is the continuum electron energy in the center-of-mass frame and the capture orbital is denoted by  $nl_j$ . In the fifth column we present the NEEC rate  $Y_n$  and in the seventh the maximum value of the convoluted cross section,  $\tilde{\sigma}_{\text{max}}$ . The last column contains total cross sections  $\sigma_{bs}$  for the competing process of bremsstrahlung.

Isotope	$E_{\text{exc}}$ (keV)	$E_c$ (keV)	$nl_j$	$Y_n$ (1/s)	$S$ (b eV)	$\tilde{\sigma}_{\text{max}}$ (b)	$\sigma_{bs}$ (b)
$^{154}_{64}\text{Gd}$	123.071	108.077	$2s_{1/2}$	$6.86 \cdot 10^7$	$8.44 \times 10^{-4}$	$3.36 \times 10^{-5}$	12.7
		108.063	$2p_{1/2}$	$1.14 \cdot 10^8$	$1.40 \times 10^{-3}$	$1.24 \times 10^{-4}$	
		108.946	$2p_{3/2}$	$1.51 \cdot 10^8$	$1.84 \times 10^{-3}$	$1.82 \times 10^{-4}$	
$^{164}_{66}\text{Dy}$	73.392	57.365	$2s_{1/2}$	$2.36 \cdot 10^7$	$1.08 \times 10^{-3}$	$4.30 \times 10^{-5}$	13.5
		57.348	$2p_{1/2}$	$1.85 \cdot 10^8$	$8.49 \times 10^{-3}$	$6.65 \times 10^{-4}$	
		58.357	$2p_{3/2}$	$2.54 \cdot 10^8$	$1.14 \times 10^{-2}$	$1.01 \times 10^{-3}$	
$^{170}_{68}\text{Er}$	78.591	61.484	$2s_{1/2}$	$2.87 \cdot 10^7$	$1.11 \times 10^{-3}$	$4.42 \times 10^{-5}$	14.3
		61.468	$2p_{1/2}$	$2.33 \cdot 10^8$	$9.04 \times 10^{-3}$	$6.26 \times 10^{-4}$	
		62.616	$2p_{3/2}$	$3.10 \cdot 10^8$	$1.18 \times 10^{-2}$	$9.30 \times 10^{-4}$	
$^{174}_{70}\text{Yb}$	76.471	58.241	$2s_{1/2}$	$9.88 \cdot 10^5$	$3.85 \times 10^{-5}$	$1.53 \times 10^{-6}$	15.2
		58.222	$2p_{1/2}$	$1.10 \cdot 10^7$	$4.30 \times 10^{-4}$	$2.63 \times 10^{-5}$	
		59.526	$2p_{3/2}$	$1.44 \cdot 10^7$	$5.48 \times 10^{-4}$	$3.91 \times 10^{-5}$	
$^{178}_{72}\text{Hf}$	93.180	73.780	$2s_{1/2}$	$3.60 \cdot 10^7$	$9.06 \times 10^{-4}$	$3.61 \times 10^{-5}$	16.0
		73.759	$2p_{1/2}$	$2.76 \cdot 10^8$	$6.94 \times 10^{-3}$	$3.79 \times 10^{-4}$	
		75.235	$2p_{3/2}$	$3.44 \cdot 10^8$	$8.47 \times 10^{-3}$	$5.43 \times 10^{-4}$	
$^{180}_{74}\text{W}$	103.557	82.939	$2s_{1/2}$	$4.22 \cdot 10^7$	$8.00 \times 10^{-4}$	$3.19 \times 10^{-5}$	16.9
		82.915	$2p_{1/2}$	$2.95 \cdot 10^8$	$5.59 \times 10^{-3}$	$2.72 \times 10^{-4}$	
		84.582	$2p_{3/2}$	$3.54 \cdot 10^8$	$6.56 \times 10^{-3}$	$3.85 \times 10^{-4}$	

a background process which may complicate the observation of NRESX. In Tables III and IV we give total radiation cross section values calculated within a nonrelativistic approximation (photon energy  $\ll$  electron rest energy) [53] for orientation. For comparison, the maximum values of the NRESX cross sections convoluted with a 10 eV width Gaussian electron energy

TABLE IV: Same as Table III for isotopes with  $M1$  nuclear transitions.

Isotope	$E_{\text{exc}}(\text{keV})$	$E_c(\text{keV})$	$nl_j$	$Y_n(1/s)$	$S$ (b eV)	$\tilde{\sigma}_{\text{max}}$ (b)	$\sigma_{bs}$ (b)
$^{155}_{64}\text{Gd}$	60.008	45.014	$2s_{1/2}$	$3.12 \cdot 10^8$	$2.61 \times 10^{-2}$	$1.04 \times 10^{-3}$	12.7
		45.001	$2p_{1/2}$	$8.37 \cdot 10^7$	$7.01 \times 10^{-3}$	$6.22 \times 10^{-4}$	
		45.883	$2p_{3/2}$	$8.39 \cdot 10^7$	$6.89 \times 10^{-3}$	$6.82 \times 10^{-4}$	
$^{165}_{67}\text{Ho}$	94.700	78.138	$2s_{1/2}$	$2.00 \cdot 10^9$	$6.75 \times 10^{-2}$	$2.69 \times 10^{-3}$	13.9
		78.122	$2p_{1/2}$	$2.71 \cdot 10^8$	$9.17 \times 10^{-3}$	$6.73 \times 10^{-4}$	
		79.198	$2p_{3/2}$	$1.47 \cdot 10^8$	$4.89 \times 10^{-3}$	$4.08 \times 10^{-4}$	
$^{173}_{70}\text{Yb}$	78.647	60.417	$2s_{1/2}$	$1.18 \cdot 10^9$	$6.85 \times 10^{-2}$	$2.73 \times 10^{-3}$	15.2
		60.398	$2p_{1/2}$	$2.67 \cdot 10^8$	$1.54 \times 10^{-2}$	$9.40 \times 10^{-4}$	
		61.702	$2p_{3/2}$	$2.17 \cdot 10^8$	$1.22 \times 10^{-2}$	$8.70 \times 10^{-4}$	
$^{175}_{71}\text{Lu}$	113.804	94.995	$2s_{1/2}$	$4.04 \cdot 10^8$	$9.72 \times 10^{-3}$	$3.87 \times 10^{-4}$	15.6
		94.975	$2p_{1/2}$	$1.39 \cdot 10^8$	$3.35 \times 10^{-3}$	$1.94 \times 10^{-4}$	
		96.363	$2p_{3/2}$	$1.32 \cdot 10^8$	$3.13 \times 10^{-3}$	$2.12 \times 10^{-4}$	
$^{179}_{72}\text{Hf}$	122.791	103.391	$2s_{1/2}$	$1.07 \cdot 10^9$	$2.26 \times 10^{-2}$	$9.00 \times 10^{-4}$	16.0
		103.370	$2p_{1/2}$	$2.06 \cdot 10^8$	$4.34 \times 10^{-3}$	$2.37 \times 10^{-4}$	
		104.846	$2p_{3/2}$	$1.39 \cdot 10^8$	$2.90 \times 10^{-3}$	$1.86 \times 10^{-4}$	
$^{185}_{75}\text{Re}$	125.35	104.112	$2s_{1/2}$	$4.74 \cdot 10^9$	$1.11 \times 10^{-1}$	$4.42 \times 10^{-3}$	17.4
		104.086	$2p_{1/2}$	$6.15 \cdot 10^8$	$1.43 \times 10^{-2}$	$6.60 \times 10^{-4}$	
		105.857	$2p_{3/2}$	$2.22 \cdot 10^8$	$5.11 \times 10^{-3}$	$2.84 \times 10^{-4}$	
$^{187}_{75}\text{Re}$	134.24	112.996	$2s_{1/2}$	$4.20 \cdot 10^9$	$8.17 \times 10^{-2}$	$3.25 \times 10^{-3}$	17.4
		112.970	$2p_{1/2}$	$5.21 \cdot 10^8$	$1.01 \times 10^{-2}$	$4.60 \times 10^{-4}$	
		114.741	$2p_{3/2}$	$1.68 \cdot 10^8$	$3.22 \times 10^{-3}$	$1.79 \times 10^{-4}$	

distribution are given ( $\tilde{\sigma}_{\text{max}}$ ). Bremsstrahlung cross sections are typically 4-6 orders of magnitude larger than the NRESX cross sections at resonance. However, since the lifetime of the NRESX process is dominated by long nuclear mean-lives, it occurs on a much longer time scale than bremsstrahlung. This fact may be exploited in a possible observation of nuclear-resonant electron scattering.

Regarding the possible experimental observation of NRES, the high sensibility of electron

TABLE V: Resonance strengths  $S$  for NRESX with capture into the  $L$ - and  $M$ -shell  $p$  orbitals of He-like ions followed by the intra-shell or  $L\alpha$  radiative decay to the  $2s$  state and IC of the bound electron. The nuclear transition multipolarity is  $E2$ .  $E_{\text{exc}}$  denotes the nuclear excitation energy,  $E_c$  is the continuum electron energy in the center-of-mass frame and  $nl_j$  stands for the capture orbital.

Isotope	$E_{\text{exc}}(\text{keV})$	$nl_j$	$E_c(\text{keV})$	$S$ (b eV)	$nl_j$	$E_c(\text{keV})$	$S$ (b eV)
$^{232}_{90}\text{Th}$	49.369	$2p_{1/2}$	18.517	0.337	$3p_{1/2}$	36.101	0.059
$^{232}_{90}\text{Th}$	49.369	$2p_{3/2}$	22.270	0.291	$3p_{3/2}$	37.223	0.064
$^{236}_{92}\text{U}$	45.242	$2p_{1/2}$	12.688	0.894	$3p_{1/2}$	31.270	0.125
$^{236}_{92}\text{U}$	45.242	$2p_{3/2}$	16.872	0.683	$3p_{3/2}$	32.519	0.131
$^{238}_{92}\text{U}$	44.916	$2p_{1/2}$	12.362	1.049	$3p_{1/2}$	30.941	0.144
$^{238}_{92}\text{U}$	44.916	$2p_{3/2}$	16.540	0.797	$3p_{3/2}$	32.190	0.151
$^{248}_{96}\text{Cm}$	43.380	$2p_{1/2}$	7.210	3.411	$3p_{1/2}$	27.927	0.306
$^{248}_{96}\text{Cm}$	43.380	$2p_{3/2}$	12.376	1.910	$3p_{3/2}$	29.469	0.299

spectrometry to strong magnetic fields restricts the choice of the experimental setup. The presence of magnetic fields in electron coolers of storage rings perturbs the electron trajectory and makes the detection of scattered electrons very difficult. At the storage ring facility at the GSI, electron scattering experiments have been performed using a gas target as electron target [39, 54, 55]. The accelerated ions are cycling in the Experimental Storage Ring (ESR) with velocities close to the speed of light and are passing through a gas target with electron densities of  $10^{12} - 10^{14}$  electrons per  $\text{cm}^2$ . The quasifree electrons are then scattered by the highly charged ions. The main drawback related to the use of gas targets is the nuclear Coulomb excitation that occurs due to the target nuclei.

For an envisaged NRES experiment, when the resonance energy condition is fulfilled, the quasifree electrons can be captured by the fast ion with the simultaneous excitation of the nucleus, being then carried away from the gas target. After a time interval corresponding to the mean lifetime of the nuclear excited state in the actual electronic configuration of the highly charged ion, the electron is expelled by the ion and can be detected using an electron spectrometer [54]. The energy of the electron will be given by the transformation of the final

continuum electron energy  $E_c$  from the center-of-mass frame to the laboratory frame [41],

$$E_c^{lab}/c = \gamma(E_c^{cm}/c + \beta p^{cm} \cos\theta). \quad (25)$$

The emitted electron is characterized in the center-of-mass system by the momentum  $p^{cm}$  with a direction determined by the polar angle  $\theta$  with respect to the  $z$  axis. In the equation above,  $c$  stands for the speed of light and  $\beta$  and  $\gamma$  are the reduced velocity and the Lorentz factor of the ion, respectively. The electron spectrometer actually detects the electrons emitted in the forward direction [54, 55].

The initial and final states of the scattering process in this scenario are the same as the ones of the non-resonant process of electron capture to the continuum (ECC) [56, 57, 58]. This process is one of the major sources of background for NRES, and due to the identical initial and final states, quantum interference between the two processes may occur. However, an investigation of the corresponding time scales for the two processes reveals that in contrast to the nuclear lifetime-dependent NRES, ECC occurs much faster. Time-discrimination spectroscopy, as it has been proposed in Ref. [35] for NEEC followed by  $\gamma$  decay of the nucleus, can therefore reduce substantially the ECC background. Similarly to the concept presented in Ref. [35], the different time scales of NRES and ECC have as a result a spatial separation of the electron emissions in a storage ring experiment. While the ECC photons will be emitted almost instantaneously in the region of the gas target, internal conversion will only occur later, after the ions have already travelled a certain distance in the ring. For the present electron spectrometer, where all forward-emitted electrons are detected approximately 90 cm after the gas target [54, 55], the separation of the signal and background events is challenging and requires a special extension of the experimental setup.

Particularly interesting is the case of NRESX occurring into the  $2p$  orbitals of He-like ions of heavy actinides, with resonance strengths presented in Table V. The captured electron undergoes a fast x-ray decay to the  $2s_{1/2}$  orbital (the decay rates are  $1.95 \times 10^{10} \text{ s}^{-1}$  for the  $2p_{1/2} \rightarrow 2s_{1/2}$  transition and  $8.86 \times 10^{14} \text{ s}^{-1}$  for the  $2p_{3/2} \rightarrow 2s_{1/2}$  transition). The IC rate for the  $2s$  orbital electron is much smaller than the one for  $2p$  orbital electrons, so that the nuclear lifetime in the case of the  $1s^2 2s$  configuration is longer than the one for the  $1s^2 2p$  capture configurations. The nuclear mean-lives of the  $1s^2 2s$  ion configuration of the four studied heavy actinides have values between  $\tau=13 \text{ ns}$  for  $^{248}_{96}\text{Cm}$  and  $\tau=50 \text{ ns}$  for  $^{232}_{90}\text{Th}$ , corresponding to a spatial separation of approximately 13 to 50 cm.

#### IV. SUMMARY

We have considered nuclear-resonant electron scattering, i.e. nuclear excitation by electron capture followed by internal conversion, focusing on finding prospective isotopes for a possible experimental observation of the process. Theoretical total cross sections and resonance strengths for a number of capture scenarios and collision systems have been presented.

In the first place, we have investigated the process of NRES involving  $E2$  and  $M1$  nuclear transitions with electron recombination into the electronic ground state. A comparison with resonance strengths for NEEC followed by the radiative decay of the nucleus shows that the two processes are typically on the same order of magnitude. For the specific cases of the heavy actinides studied, the IC nuclear decay channel prevails, and the NRES resonance strengths are between one and two orders of magnitude larger.

A second scenario in which the electronic capture occurs into an excited electronic state and is followed by x-ray emission has also been investigated. Due to the large width of the excited electronic state, the continuum electron resonance energy condition is significantly relaxed. We have found that for the heavy actinide isotopes, NRESX with electronic capture and IC from different subshells of the  $L$  shell presents large resonance strength values. Furthermore, the possible experimental observation of NRES in storage rings, e.g. at the present and future ESR facility of the GSI Darmstadt has been discussed, devoting special attention to the electron target setup. A time-discrimination measurement at the ESR could be used for discerning the process of NRES from the background of other atomic physics processes, such as ECC. The most promising candidates for time-discrimination measurements were found to be the heavy actinide nuclei in a NRESX scenario involving the  $L$ -shell orbitals. While the calculated resonance strengths, on the order of 1 b eV, still make the observation of the NRES effect challenging, the advent of the new storage ring facility at GSI and the reported interest for electron spectroscopy experiments in the relativistic regime are strong arguments for the need of consistent theoretical predictions and experimental scenarios.

## Acknowledgments

The authors would like to thank Alexander Voitkiv for helpful comments. A.P. is indebted to Stefan Schippers, Siegbert Hagmann and Christophor Kozhuharov for discussions concerning the experimental issues mentioned in this paper.

- 
- [1] I. D. Williams, Rep. Prog. Phys. **62**, 1431 (1999).
  - [2] K. Bartschat, Comput. Phys. Commun. **114**, 168 (1998).
  - [3] C. P. Bhalla and R. Shingal, J. Phys. B **24**, 3187 (1991).
  - [4] W. R. Johnson and C. Guet, Phys. Rev. A **49**, 1041 (1994).
  - [5] R. Shingal, Z. Chen, K. R. Karim, C. D. Lin, and C. P. Bhalla, J. Phys. B **23**, L637 (1990).
  - [6] T. J. M. Zouros, E. P. Benis, and T. W. Gorczyca, Phys. Rev. A **68**, 010701(R) (2003).
  - [7] E. P. Benis, T. J. M. Zouros, T. W. Gorczyca, A. D. González, and P. Richard, Phys. Rev. A **69**, 052718 (2004).
  - [8] S. R. Grabbe, G. Tóth, C. P. Bhalla, and P. Richard, Nucl. Instrum. Meth. B **124**, 347 (1997).
  - [9] P. Richard, C. P. Bhalla, S. Hagmann, and P. A. Závodszky, Physica Scripta **T80**, 87 (1999).
  - [10] J. B. Greenwood, I. D. Williams, and P. McGuinness, Phys. Rev. Lett. **75**, 1062 (1995).
  - [11] C. Bélenger, P. Defrance, R. Friedlein, C. Guet, D. Jalabert, M. Maurel, C. Ristori, J. C. Rocco, and B. A. Huber, J. Phys. B **29**, 4443 (1996).
  - [12] B. A. Huber, C. Ristori, P. A. Hervieux, M. Maurel, C. Guet, and H. J. Andrä, Phys. Rev. Lett. **67**, 1407 (1991).
  - [13] P. H. Janzen, L. D. Gardner, D. B. Reisenfeld, D. W. Savin, J. L. Kohl, and K. Bartschat, Phys. Rev. A **59**, 4821 (1999).
  - [14] J. Jiang, C. Z. Dong, L. Y. Xie, J. Wang, J. Yan, and S. Fritzsche, Chin. Phys. Lett. **24**, 691 (2007).
  - [15] T. Y. Suzuki, H. Suzuki, F. J. Currell, S. Ohtani, Y. Sakai, T. Takayanagi, and K. Wakiya, Phys. Rev. A **57**, 1832 (1998).
  - [16] B. Wallbank, N. Djuric, O. Voitke, S. Zhou, G. H. Dunn, A. C. H. Smith, and M. E. Bannister, Phys. Rev. A **56**, 3714 (1997).
  - [17] A. Itoh, T. J. M. Zouros, D. Schneider, U. Settner, and N. Stolterfoht, J. Phys. B **18**, 4581

- (1985).
- [18] N. R. Badnell, Phys. Rev. A **41**, 3555 (1990).
  - [19] K. Kollmar, N. Grün, and W. Scheid, Europhys. J. D **10**, 27 (2000).
  - [20] C. W. De Jager, H. De Vries, and C. De Vries, At. Data Nucl. Data Tabl. **14**, 479 (1974).
  - [21] H. De Vries, C. W. De Jager, and C. De Vries, At. Data Nucl. Data Tabl. **36**, 495 (1987).
  - [22] A. Pálffy, W. Scheid, and Z. Harman, Phys. Rev. A **73**, 012715 (2006).
  - [23] V. I. Goldanskii and V. A. Namiot, Phys. Lett. **62B**, 393 (1976).
  - [24] T. Carreyre, M. R. Harston, M. Aiche, F. Bourguine, J. F. Chemin, G. Claverie, J. P. Goudour, J. N. Scheurer, F. Attallah, G. Bogaert, et al., Phys. Rev. C **62**, 024311 (2000).
  - [25] S. Kishimoto, Y. Yoda, M. Seto, Y. Kobayashi, S. Kitao, R. Haruki, T. Kawauchi, K. Fukutani, and T. Okano, Phys. Rev. Lett. **85**, 1831 (2000).
  - [26] D. Kekez, A. Ljubičić, K. Pisk, and B. A. Logan, Phys. Rev. Lett. **55**, 1366 (1985).
  - [27] P. Kálmán, Phys. Rev. A **43**, 2603 (1991).
  - [28] P. Kálmán and T. Bükki, Phys. Rev. C **63**, 027601 (2001).
  - [29] M. R. Harston and J. F. Chemin, Phys. Rev. C **59**, 2462 (1999).
  - [30] N. Cue, J.-C. Poizat, and J. Remillieux, Eurphys. Lett. **8**, 19 (1989).
  - [31] J. Kimball, D. Bittle, and N. Cue, Phys. Lett. **152**, 367 (1991).
  - [32] Z.-S. Yuan and J. C. Kimball, Phys. Rev. C **47**, 323 (1993).
  - [33] A. Pálffy, Z. Harman, and W. Scheid, Phys. Rev. A **75**, 012709 (2007).
  - [34] A. Pálffy, Z. Harman, A. Surzhykov, and U. D. Jentschura, Phys. Rev. A **75**, 012712 (2007).
  - [35] A. Pálffy, Z. Harman, C. Kozhuharov, C. Brandau, C. H. Keitel, W. Scheid, and T. Stöhlker, Phys. Lett. B **661**, 330 (2008).
  - [36] C. Brandau, T. Bartsch, A. Hoffknecht, H. Knopp, S. Schippers, W. Shi, A. Müller, N. Grün, W. Scheid, T. Steih, et al., Phys. Rev. Lett. **89**, 053201 (2002).
  - [37] C. Brandau, C. Kozhuharov, A. Müller, W. Shi, S. Schippers, T. Bartsch, S. Böhm, C. Böhme, A. Hoffknecht, H. Knopp, et al., Phys. Rev. Lett. **91**, 073202 (2003).
  - [38] Facility for Antiproton and Ion Research Homepage, <http://www.gsi.de/fair>.
  - [39] S. Hagmann, T. Stöhlker, C. Kozhuharov, J. Ullrich, R. Dörner, R. Moshhammer, M. Nofal, H. Rothard, U. Spillmann, R. Reuschl, et al., Nucl. Instrum. Meth. B **261**, 218 (2007).
  - [40] W. Greiner and J. A. Maruhn, *Nuclear Models* (Springer Verlag Berlin Heidelberg, 1996).
  - [41] J. Eichler and W. Meyerhof, *Relativistic Atomic Collisions* (Academic Press San Diego, 1995).

- [42] S. Raman, C. Nestor, and P. Tikkanen, *At. Data Nucl. Data Tabl.* **78**, 1 (2001).
- [43] C. W. Reich, *Nucl. Data Sheets* **71**, 709 (1994).
- [44] L. K. Peker, *Nucl. Data Sheets* **65**, 439 (1992).
- [45] V. S. Shirley, *Nucl. Data Sheets* **54**, 589 (1988).
- [46] M. S. Basunia, *Nucl. Data Sheets* **102**, 719 (2004).
- [47] G. Baglin, *Nucl. Data Sheets* **72**, 617 (1994).
- [48] E. Browne, *Nucl. Data Sheets* **74**, 165 (1995).
- [49] R. Firestone, *Nucl. Data Sheets* **62**, 159 (1991).
- [50] P. Ring and P. Schuck, *The Nuclear Many-Body Problem* (Springer Verlag New York, 1980).
- [51] F. A. Parpia, C. Froese-Fischer, and I. P. Grant, *Comp. Phys. Comm.* **94**, 249 (1996).
- [52] W. R. Phillips, I. Ahmad, D. W. Banes, B. G. Glagola, W. Henning, W. Kutschera, K. E. Rehm, J. P. Schiffer, and T. F. Wang, *Phys. Rev. Lett.* **62**, 1025 (1989).
- [53] H. W. Koch and J. W. Motz, *Rev. Mod. Phys.* **31**, 920 (1959).
- [54] S. Hagmann, T. Stöhlker, J. Ullrich, C. Kozhuharov, R. Moshhammer, H. Kollmus, R. Mann, and M. Nofal, *Nucl. Instrum. Meth. B* **205**, 207 (2003).
- [55] M. Nofal, S. Hagmann, T. Stöhlker, D. J.-A. C. Kozhuharov, X. Wang, A. Gumberidze, U. Spillmann, R. Reuschl, S. Hess, S. Trotsenko, et al., *Phys. Rev. Lett.* **99**, 163201 (2007).
- [56] G. B. Crooks and M. E. Rudd, *Phys. Rev. Lett.* **25**, 1599 (1970).
- [57] L. Sarkadi, J. Pálinkás, A. Kövér, D. Berényi, and T. Vajnai, *Phys. Rev. Lett.* **62**, 527 (1989).
- [58] D. H. Jakubassa-Amundsen, *Rad. Phys. Chem.* **75**, 1319 (2006).